International Journal of Thermophysics, Vol. 14, No. 3, 1993

Pulsed Laser Melting and Resolidification of Metal Silicide Layers[1]

P. Baeri,[2] M. G. Grimaldi,[2] F. La Via,[3] C. Spinella,[3] and G. Spoto[4]

Ti, Fe, and Co silicide layers, 80–200 nm thick, on top of single crystal silicon substrate have been melted by 25-ns ruby laser pulses and the resolidified structures have been analyzed by transmission electron microscopy, X-ray diffraction, and Rurtherford backscattering spectrometry. Metastable phases and/or epitaxial layers are obtained upon solidifcation. The transient molten layer has been monitored by means of time-resolved optical measurements with nanosecond resolution; in all cases solidification velocity of the order of $1\ m \cdot s^{-1}$ was observed, and in one case liquid undercooling as much as 800 K was estimated.

KEY WORDS: laser pulse; silicide; melting; phase transition; solidification.

1. INTRODUCTION

Melting thin surface layers (10–100 nm) by irradiation with a pulse (10-100-ns) high-power laser beam has the following three major features. (a) Heating rates of the order of $10^{11}\ K \cdot s^{-1}$ prevent any solid-state reaction or decomposition prior of melting so that metastable phases are brought to their metastable melting point. (b) The melt lasts some hundred nanoseconds. This is long enough to produce considerable diffusion of atoms in liquid phase (mixing) over the film thickness. (c) Due to the high temperature gradient created by the laser shot, the heat flux toward the bulk (almost $10^7\ W \cdot cm^{-2}$) imposes a solidification velocity of the order of

[1] Paper presented at the Third Workshop on Subsecond Thermophysics, September 17–18, 1992, Graz, Austria.

[2] Dipartimento di Fisica, Università di Catania, Corso Italia 57, 195129 Catania, Italy.
[3] IMETEM CNR Stradale Primosole 50, 195121 Catania, Italy.
[4] Dipartimento di Chimica, Università di Catania, Via A. Doria, 195125 Catania, Italy.

0195-928X/93/0500-0383$07.00/0

several meters per second and/or severe supercooling of the liquid layer, both conditions leading to quenching of metastable phases. The reader can find several examples concerning these features in some review papers concerning both the semiconductors [1] and the metallic systems [2]. The method is often called pulsed laser annealing (PLA). In the present paper we show some examples related to the PLA formation of metal silicide layers on top of a single crystal silicon substrate.

Silicide layers are currently prepared in the solid phase by thermal treatment of metal films deposited on top of silicon substrates mainly for constructing semiconductor devices.

The alternative method of PLA for growing silicide layers presents some useful practical advantages for device production. Since PLA induces so far fastest liquid-to-solid transitions, it represents a frontier method to verify any theory related to far from equilibrium phase transitions.

Major features of so-formed silicide layers are metastability and/or epitaxy. In this paper we show examples of PLA formation of titanium, iron, and cobalt disilicides. The first two cases (Ti and Fe) are examples of metastable phases formation; in the Co case, instead a stable phase is formed after PLA but the liquid phase epitaxial regrowth on the silicon substrate has some interesting features. The time-resolved reflectivity (TRR) is discussed in conjunction with results in the case of $TiSi_2$ and $CoSi_2$. This method permits the monitoring of the melting-solidification dynamics through the different optical constants of the solid and the liquid phase.

We show that the features of the time-resolved reflectivity signal during the irradiation of $TiSi_2$ layers allowed evaluation of the supercooling of the liquid layer and observation of the homogeneous nucleation of a metastable phase. In the case of $CoSi_2$, instead, TRR allowed evaluation of the solidification velocity.

2. EXPERIMENTS

Laser irradiations were performed in air with single-shot, 25-ns ruby laser pulses (694-nm wavelength) with energy densities ranging from 0.2 to 1 $J \cdot cm^{-2}$. The irradiated area was homogeneous within 5% over a circular spot 3 mm in diameter.

The irradiated targets were thermally grown polycrystalline $TiSi_2$, $FeSi_2$, and $CoSi_2$ layers, 80–200 nm thick, on top of Si (100)- or (111)-oriented single crystal substrates.

Time-resolved reflectivity signals were detected by a fast pin photodiode and a storage oscilloscope with 2-ns overall resolution. The incident beam for TRR came from a 15-mW Argon laser (488-nm wavelength)

focused on the sample surface at the center of the area irradiated by the ruby laser. The incidence angle was 75°.

Sample analysis after irradiation was performed by 2-MeV He Rurtherford backscattering spectrometry (RBS) and by 400-kV transmission electron diffraction (TED) and transmission electron microscopy (TEM) in a plane-view configuration. X-ray diffraction (XRD) in the Bragg–Bentano configuration was also used in the case of polycrystalline films, using Cu–K_α radiation.

3. RESULTS

3.1. $TiSi_2$

$TiSi_2$ is known to exist in two orthorombic phases, namely, the C54 face centered structure, which is a prototype structure with lattice parameters $a = 0.825$ nm, $b = 0.478$ nm, and $c = 0.854$ nm [3], and the C49 body centered ZrSi2-type structure, with lattice parameters $a = 0.356$ nm, $b = 1.361$ nm, and $c = 0.356$ nm [4].

The first one is the stable phase reported in the assessed Ti–Si phase diagram with a congruent melting point at 1500°C and a peritectic decomposition predicted at 1330°C. The second one is a metastable phase which was formed by low-temperature annealing of amorphous codeposited Ti–Si films and is transformed to the stable C54 phase after annealing at 650°C [4]. The phase expected for near-equilibrium solidification of a liquid stoichiometric $TiSi_2$ mixture is the C54 face centered orthorombic one.

Our starting sample was a polycrystalline, 200-nm-thick film of C54 $TiSi_2$ obtained by high-temperature rapid thermal treatment of Ti films deposited on (100)-oriented silicon single crystal [5]. The correct stoichiometry of the film was tested by RBS, which also revealed a flat and uniform silicide/Si interface. The diffraction pattern of this film is reported in Fig. 1, where several rings are identified as belonging to plane spacings of the C54 phase. The right in Fig. 1 is a TEM micrograph showing the randomly oriented grains with an average size of 400 nm.

Samples were then irradiated with different energy density shorts. For irradiation at $1.0\ J \cdot cm^{-2}$, all of the silicide layer was melted, but not (or very scarcely) the underlying substrate. At lower energy densities the silicide layer was only partially melted and at higher energy densities considerable interdiffusion in liquid phase took place between the silicide and the silicon substrate as revealed by RBS analysis.

The resolidified layer after $1.0\ J \cdot cm^{-2}$ irradiation showed (Fig. 2, right) a very fine-grain structure with an average size of about 20 nm, and the diffraction rings (Fig. 2, left) clearly do not match the righs of the C54

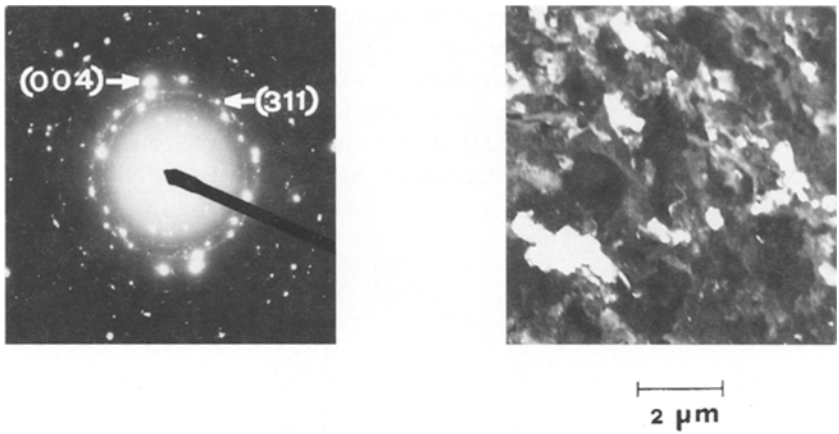

Fig. 1. TED diffraction pattern (left) and TEM image (right) of 200-nm-thick C54 $TiSi_2$ film thermally grown on a Si substrate.

phase. They are instead recognized as belonging to the C49 phase. In particular, the hardly resolved rings corresponding to the 0.227-nm (060) and the 0.222-nm (131) lattice spacings, and the inner one corresponding to the 0.34-nm (040) lattice spacing unambiguously identifies the C49 phase.

Phase stability was checked by isochronal (30-min) thermal annealing in a vacuum furnace. In Fig. 3 the XRD spectra of the as-prepared sample,

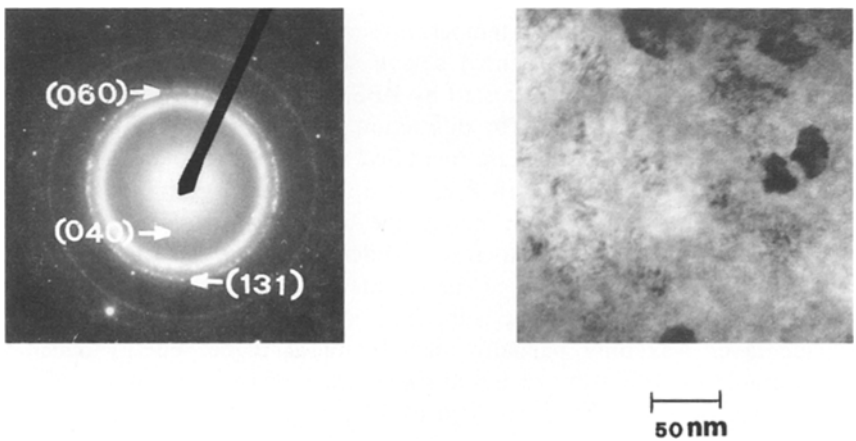

Fig. 2. TED diffraction pattern (left) and TEM image (right) of 200-nm-thick C49 $TiSi_2$ film obtained by PLA.

after PLA treatment and after annealing at different temperatures, are reported. The as-prepared sample (Fig. 3a) shows peaks corresponding to the (311), (004), and (022) interplanar spacing of the C54 phase. No peak is seen following PLA (Fig. 3b) since, as seen by TEM, crystallites are too small to produce visible X-ray diffraction peaks. After annealing at 200, 400, and 600°C (Figs. 3c, d, e), samples showed progressively increasing

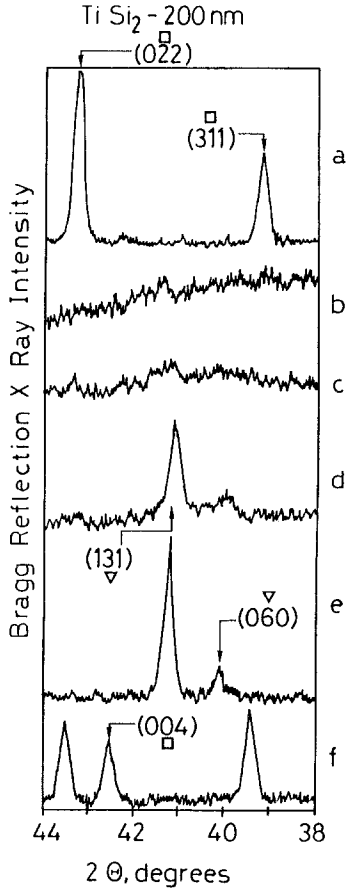

Fig. 3. XRD spectra of thermally grown $TiSi_2$ film (a), after PLA (b), and after further annealing at 200°C (c), 400°C (d), 600°C (e), and 700°C (f). Squares and triangles mark peaks related to the C54 and C49 phaser, respectively.

peaks identified as corresponding to the (060) and (311) interplanar spacings of the C49 phase. After 700°C annealing these peaks disappeared and those previously recognized as belonging to the C54 phase appeared again (Fig. 3f). This result clearly confirms that the phase formed upon PLA is the metastable C49 phase of $TiSi_2$, which is well-known to decay into the stable C54 $TiSi_2$ phase upon thermal annealing at 650°C [6].

We stress the fact that because of competition between the growth kinetics in the solid phase of the C54 and C49 phases, it is very dificult to produce a $TiSi_2$–C49 phase film as thick as the present one.

The reflectivity vs time signal registered during the 1.0 $J \cdot cm^{-2}$ irradiation is shown in Fig. 4. For comparison, the reflectivity signal for a pure silicon sample with a comparable melt time duration is also reported in Fig. 4 (bottom). The time evolution of the ruby laser pulse is also reported as a dashed line. The liquid reflectivity is higher than the solid one for both Si and $TiSi_2$. In both cases, the reflectivity increases from the solid to the liquid value when the ruby pulse is at its peak intensity, indicating the start of surface melting.

In pure silicon, a planar liquid solid interface which moves toward the inner sample and then comes back to the surface results after laser

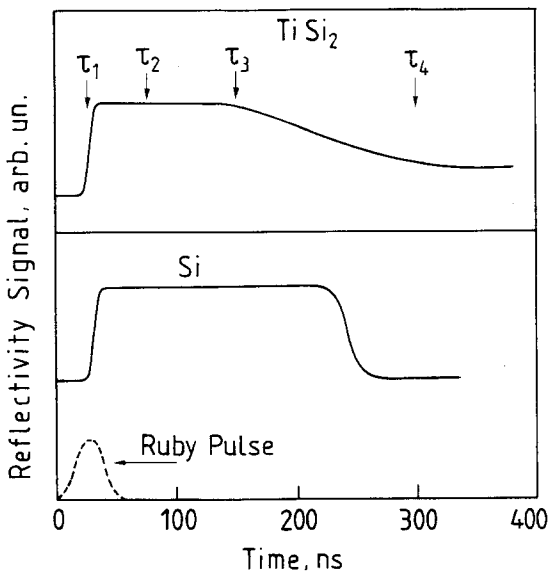

Fig. 4. Top: TRR trace registered during PLA of 200-nm-thick $TiSi_2$ film on top of a Si substrate. Bottom: The same for a pure Si sample. Dashed line: time evolution of the laser pulse used for PLA.

irradiation [7]. The entire movement is not seen by the probe light on account of its extinction length in the liquid, so that only the outermost 10 nm of the sample is probed.

The decrease in the reflectivity signal (about 200 ns after its rise) is then related to the surface solidification, which in the case of Si lasts for about 10 ns (i.e., the time needed for the signal to decay from the liquid to the solid value). From this time, the liquid–solid interface velocity can be estimated to be of the order of $1\ \mathrm{m \cdot s^{-1}}$. A quite different signal is seen for the $TiSi_2$ irradiation. In fact, although the overall duration of the signal is almost the same as for Si, the solidification time (between instant τ_3 and instant τ_4 marked by arrows in Fig. 4) is about 150 ns, which is more than one order of magnitude greater then that of the pure Si case. This would imply a liquid–solid interface velocity lower than $0.1\ \mathrm{m \cdot s^{-1}}$, which is obviously in contrast to the whole signal duration of 250 ns. In fact, at this velocity the time required for the solidification of the 200-nm-thick layer would be more than 2 μs. This analysis excludes the solidification of the molten $TiSi_2$ layer to proceed via a planar liquid–solid interface and suggests, instead, that the measured 150-ns solidification time is due to the random nucleation and growth inside the liquid of the crystallites seen in the TEM micrograph in Fig. 2. From Fig. 2 a crystallite nuclei density of the order of $10^{18}\ \mathrm{cm^{-3}}$ is observed, and from Fig. 4 the nucleation time was about 100 ns, so that a value of $10^{25}\ \mathrm{s^{-1}}$ for the nucleation rate is derived. Such a value, following the standard theory of nucleation, must be related to a considerable liquid undercooling. The liquid had to be undercooled with respect both to its equilibrium temperature with the C54 phase and top its equilibrium temperature with the C49 phase in order to allow for such copious nucleation of crystallite from the melt. The reflectivity signal allows evaluation of the degree of undercooling. In fact, assuming an entalpy release of $12.1\ \mathrm{kcal \cdot mol^{-1}}$ during the 150-ns solidification time of the 200-nm $TiSi_2$ layer, the heat flow toward the bulk would be $1.5 \cdot 10^6\ \mathrm{W \cdot cm^{-2}}$. This value is in perfect agreement with the one evaluated by heat flow computation [7]. Moreover, the plateau region of the reflectivity signal (between instant τ_1 and instant τ_3 marked by arrows in Fig. 4) can be divided into two regions: the first one (between τ_1 and τ_2) lasts about 50 ns and it represents the time needed for the melt front to reach the silicon substrate. The correct value of 50 ns is predicted by heat flow calculations [8] and it roughly coincides with that portion of the signal overlapped with the heating pulse. The remaining 70 ns (between τ_2 and τ_3 in Fig. 4) represents the time during which the liquid layer is cooled before nucleation of the crystallites occurs. With the previously determined value of heat flow toward the bulk, the liquid temperature at instant τ_3 is estimated to be 800 K below the melting temperature of the C54 phase.

3.2. $FeSi_2$

Very recently, considerable efforts have been devoted to the study of the Fe–Fi system because of the existence of a semiconducting $FeSi_2$ phase (β phase) which has a distorted fluorite structure (orthorhombic $a = 0.986$ nm, $b = 0.779$ nm, and $c = 0.783$ nm). It should be of practical relevance to build up epitaxial $\beta FeSi_2$ layers on top of silicon for the preparation of optoelectronic devices [9]. More recently, epitaxial $\beta FeSi_2$ layers have been obtained in the solid phase but with a limited thickness (< 30 nm). Following laser melting and resolidification of $FeSi_2$ layers, liquid phase epitaxy could be achieved, although it is a noncongruent compound as in the case of NiSi2, even for thicker films; so we attempted it. Our starting sample was a polycrystalline $\beta FeSi_2$ film 80 nm thick on top of a (111)-oriented silicon wafer obtained by conventional thermal treatment of Fe layers deposited on Si. The electron diffraction pattern from such a film is shown in Fig. 5 (spots refer to the underlying silicon). Two families of planes are recognized as corresponding to (113) and (114) plane spacings of 0.24 and 0.186 nm, respectively. After PLA with 0.8 $J \cdot cm^{-2}$ irradiation, the whole silicide layer was melted, but not the underlying

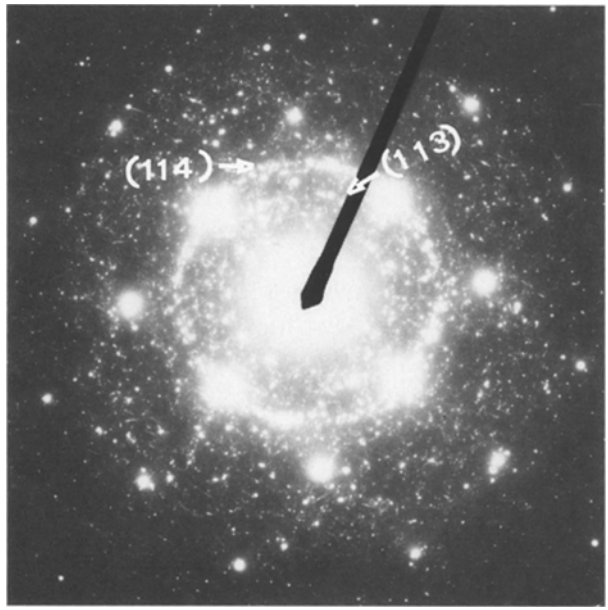

Fig. 5. TED pattern from a thermally grown 80-nm-thick $FeSi_2$ film on a Si substrate. Spots are the [100] Si pole diffraction pattern. Identified $\beta FeSi_2$ plane families are marked by arrows.

crystal, so that, as in the case previously described for $TiSi_2$, the film stoichiometry was unchanged. To identify the phase formed by PLA, we performed TED along the [111], [110], and [114] silicon poles and the resulting patterns are reported in Figs. 6a, b, and c, respectively. No spots different from those of silicon are present along the [111] and [110] poles. Instead, along the [114] Si pole, which is diametrically opposite to the [110] pole, 35.5° away from the [111] one, the diffraction pattern of the silicide layer could be resolved (Fig. 6c). The six more intense spots belong to the silicon substrate [(220) and (113) reflections]. Superimposed on them, a regular array of diffraction spots is observed and can be explained as diffraction spots from a [110] pole of a cubic crystal having the same lattice parameter of Si.

The phase resulting from the fast quenching of a liquid $FeSi_2$ on a (111)-oriented Si crystal has therefore been unambiguously identified as a cubic epitaxial crystal, with the same lattice parameter of Si, twinned 180° about the [111] surface normal axis (so-called B-type epitaxy). Such a phase is not predicted by the phase diagram and cannot be achieved by equilibrium treatments. We tested the stability of this phase by isochronal vacuum furnace annealing. After 30 min of annealing at 700°C the cubic phase precipitated back into the $\beta FeSi_2$ phase, still maintaining an epitaxial relationship with the substrate. A TED pattern along the [111] Si pole of the precipitated sample is shown in Fig. 7. Along with the spot of the Si substrate ([111] pole), the diffraction pattern of the [101] pole of the $\beta FeSi_2$ is recognized (picture is complicated by double diffraction spots). This indicates that the whole film of $\beta FeSi_2$ obtained after precipitation from the cubic phase is epitaxial with the substrate and the (101) planes or (110) planes are parallel of the (111) silicon plane.

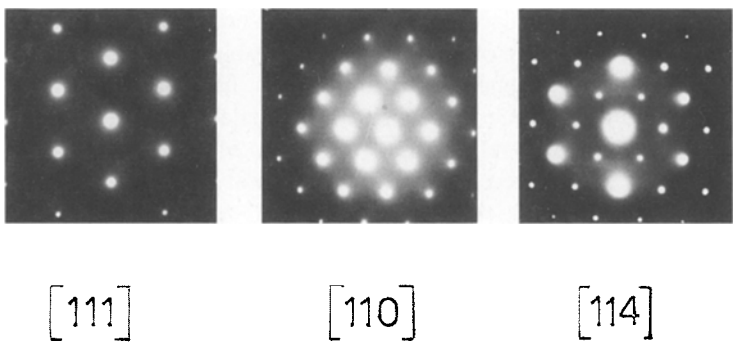

Fig. 6. TED patterns of 80-nm-thick $FeSi_2$ film on top of a (111)-oriented Si substrate obtained by PLA. a, (111) Si pole; b, (110) Si pole; c, (114) Si pole.

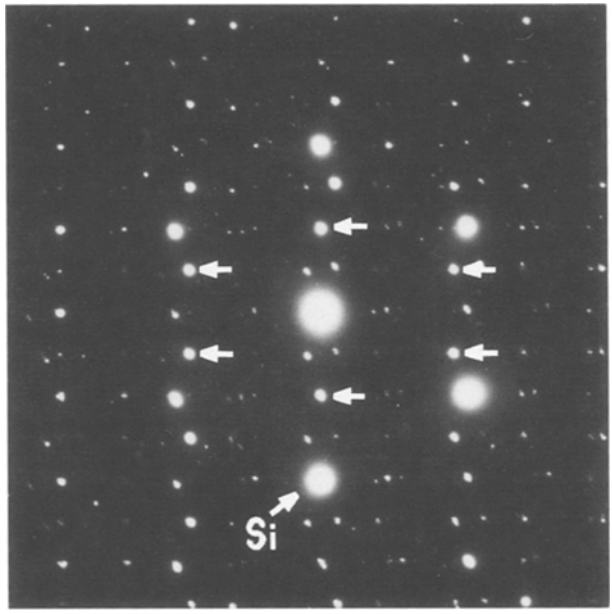

Fig. 7. TED diffraction pattern of 80-nm-thick $FeSi_2$ film on top of a (111)-oriented Si substrate obtained by PLA and subsequent 30-min, 700°C annealing. Arrows mark the main diffraction patern of the $\beta FeSi_2$ (101) pole.

3.3. $CoSi_2$

$CoSi_2$ is a congruent compound which melts at 1320°C, and it has a cubic structure with lattice constant $a = 0.543$ nm which matches that of silicon very well. Epitaxy of $CoSi_2$ is then possible, and indeed, it is easily achieved during solid phase reaction of Co films deposited on (111) Si-oriented substrates. On (110), instead, epitaxy is more difficult to achieve and only polycrystalline films have been obtained [9]. Our starting sample was, as in the preceding cases, a randomly oriented polycrystalline film of $CoSi_2$, 150 nm thick, on top of a (100)-oriented Si substrate. The diffraction pattern from this film is shown in Fig. 8 (left), where the main family planes of $CoSi_2$ is identified and marked by arrows. After PLA with the correct energy density in order to melt all through the layer but not the substrate ($0.8\ J \cdot cm^{-2}$), the film structure was changed as evidenced by the diffraction pattern shown at the right in Fig. 8. Single crystal diffraction spots are now present along the [114] Si pole. As in the case of $FeSi_2$, the smaller spots belong to the film and show that the cubic $CoSi_2$ is B-type

epitaxial. On the (100)-oriented substrate four possible equivalent [111] rotation axis exits for the crystal twinning so that the resulting film, although epitaxial, is still formed of several grains, rotated 180° around the four directions. The grains, as revelated by TEM not shown here, had an average size of 300 nm, which is much greater than that previously shown in the case of $TiSi_2$. This is not surprising since in the $CoSi_2$ case the substrate acts as seed for solid nucleation, and indeed, the time-resolved reflectivity traces, shown in Fig. 9, are similar to those of pure silicon and do not show the long tail due to the crystallite nucleation in the melt.

In Fig. 9, bottom, the calculated melt depth vs time for the 150-nm $CoSi_2$ film irradiated with $0.8\ J \cdot cm^{-2}$ is shown. The melt starts at the sample surface about at the peak of the ruby laser pulse and reaches the silicon substrate about 50 ns later, then it stops for a few nanoseconds and starts to move toward the surface. Solidification of the whole layer is achieved after 60 ns. The calculated velocity of the liquid–solid interface is $2.5\ m \cdot s^{-1}$ and the total melt time is 120 ns. This is to be compared with the experimental data for the TRR measurement, which, for the same energy density, are reported in Fig. 9, top. Both the instant of the surface melting and of the complete solidification agree with the calculated one.

In Fig. 10 the calculated melt duration for the some sample is reported as a function of the energy density of the laser shot. Calculations were performed by numerically solving the heat diffusion equation adding a heat source which represents the power density of the laser pulse absorbed by the sample and also taking into account the enthalpy release during the phase transitions with some special boundary conditions at the liquid/solid phase interfaces as described in detail elsewhere [1, 7]. Also in Fig. 10, the filled circles are the experimental values obtained by TRR measurements. The overall agreement between experiment and calculation is excellent,

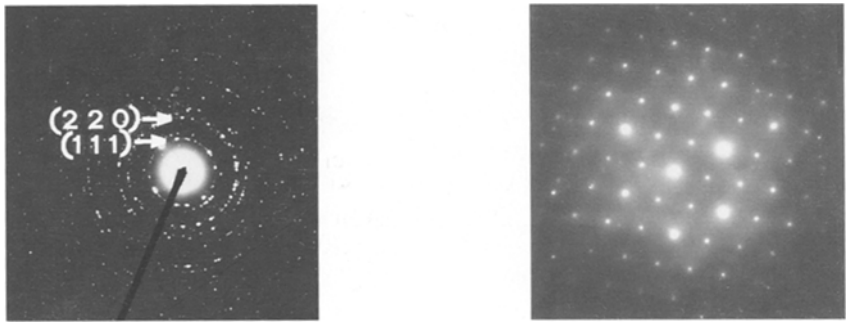

Fig. 8. Left: TED diffraction pattern of 150-nm-thick $CoSi_2$ film thermally grown on Si (100)-oriented substrate. Right: TED diffraction pattern along the (114) Si pole of the same sample after PLA.

giving us confidence in the model of a moving planar liquid–solid interface so that the calculated velocity is a very accurate evaluation. Our heat flow computations did not take into account any interface response function for the $CoSi_2$ liquid–solid interface and its movement was determined only by the energy balance between the heat flow and the enthalpy release without assuming any undercooling with respect to the equilibrium temperature between the liquid and the solid phases. This is, in principle, incorrect, but we have seen that the heat flow evaluation of the solidification dynamics is not appreciably affected by introducing an interfacial response function with some reasonable slope [1]. The reason is simply that the energy that the substrate, acting as a heat sink, must extract from the liquid layer in order to allow for the liquid supercooling is in general much lower than that required for balancing the solidification enthalpy release. For example, if we assume in the $CoSi_2$ case the same interface response function slope as for pure Si, which has been evaluated to be $15\ K \cdot s \cdot m^{-1}$ [10], the liquid should be 40 K undercooled. This means that about $3 \times 10^{-4}\ cal \cdot cm^{-2}$

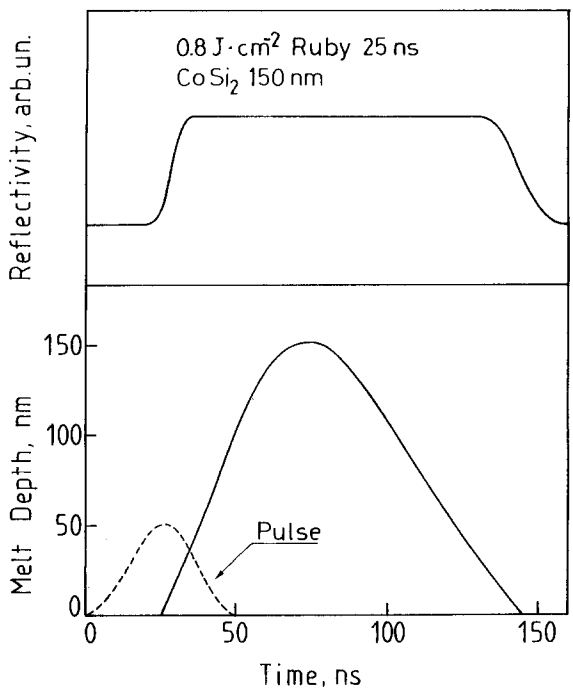

Fig. 9. Bottom: Calculated melt depth evolution for $0.8\ J \cdot cm^{-2}$, 25-ns ruby laser pulse irradiation of 150-nm-thick $CoSi_2$ film of a Si substrate. Top: Experimental TRR trace for the same case. Dashed line represents the time evolution of the laser pulse.

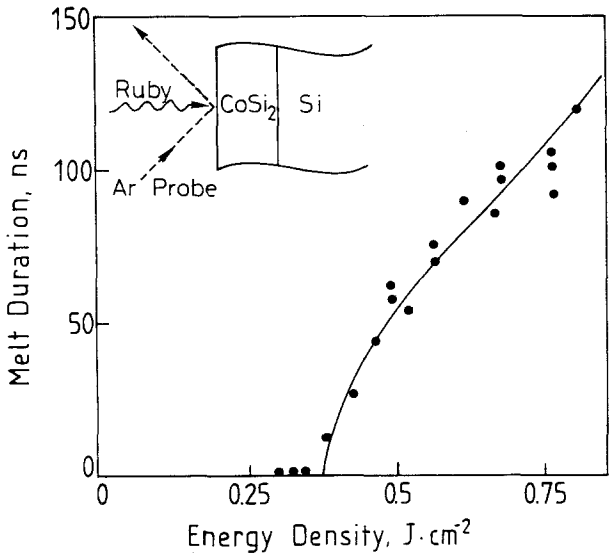

Fig. 10. Calculated melt duration vs energy density of a 25-ns ruby laser pulse irradiating a 150-nm-thick $CoSi_2$ film on a Si substrate. Filled circles represent experimental data obtained by TRR measurements.

should be extracted from the liquid layer, while the enthalpy release during the whole layer solidification is 1.5×10^{-2} cal·cm^{-2}, which is 50 times greater. In our case, in order to calculate melt durations which would be beyond the errors above the experimental data in Fig. 10, we should have assumed an interfacial response function with a slope of 50 K·s·m^{-1}. This corresponds to about 125 K undercooling.

4. SUMMARY AND CONCLUSION

We have reported data on the structure characterization of films obtained following fast solidification of liquid $TiSi_2$, $FeSi_2$, and $CoSi_2$. In all cases solidification of 100- 200-nm-thick layers takes place in a hundred nanoseconds or less, which implies a solidification velocity of the order of 1 m·s^{-1}. In the case of $CoSi_2$ and $FeSi_2$ solidification proceeds via a planar liquid–solid interface since the result is a layer having an epitaxial relationship with the substrate. For these cases heat flow computation can simulate the melt front evolution and allow a precise evaluation of the solidification velocity. We have shown a good agreement between the calculated and the experimental melt duration in the case of $CoSi_2$. Similar results, not shown herein for the sake of brevity, have been obtained for

$FeSi_2$. In both cases the undercooling of the liquid layer could, in principle, be estimated by comparing the experimental and calculaned melt front evolution. This has been done, for example, for the case of pure Si [10]. We stated only an upper limit of 125 K in the $CoSi_2$ case, which is surely a large overestimate and too rough to allow for a sufficiently accurate evaluation of the free energy level reached by the liquid layer for the purpose of more precise thermodynamical treatment. In particular, no thermodynamical or kinetic criterion for the solidification of a metastable phase is given here to understand why a metastable phase was quenched in the iron case and an equilibrium phase in the cobalt case in spite of the same quenching conditions.

A quite different melt evolution is seen in the case of $TiSi_2$. In this case, in fact, epitaxy is not allowed and the substrate does not act as seed for solid nucleation. So the liquid simply undercools until random homogeneous nucleation occurs. The cooling rate under our conditions was of the order of $10^{10}\,K \cdot s^{-1}$ and the metastable C49 $TiSi_2$ phase nucleated. We have evaluated a nucleation frequency of $10^{25}\,s^{-1}$, indicating that the liquid temperature must have been largely below the critical temperature for homogeneous nucleation, which is some hundred degrees kelvin below the melting point. Indeed, comparison of the reflectivity traces with heat flow calculations allowed us to state that the liquid $TiSi_2$ must have been 800 K supercooled below its equilibrium temperature with the equilibrium C54 phase. We have shown with some examples related to Fe, Co, and Ti disilicide that PLA is a suitable tool both for producing uniform layers of metastable phases and for studying nonequilibrium phase transition.

REFERENCES

1. P. Baeri, *Phil. Mag.* **61**:587 (1990).
2. D. M. Follstaedt, P. S. Peercy, and J. H. Perepezko, *Mat. Res. Soc. Symp. Proc.* **100**:573 (1988).
3. A. Taylor and B. J. Kagle, *Crystallographic Data on Metal and Alloy Structures* (Dover, New York, 1963).
4. R. Beyers and R. Sinclair, *J. Appl. Phys.* **57**:5250 (1985).
5. F. La Via, C. Spinella, E. Rimini, A. La Mantia, and G. Ferla, *J. Vacuum Sci. Technol.* **A7**:2609 (1989).
6. H. Kato and Y. Nakamura, *Thin Solid Film* **34**:135 (1978).
7. P. Baeri and S. U. Campisano, in *Laser Annealing of Semiconductors*, J. M. Poate and J. W. Mayer, eds. (Academic Press, New York, 1982), Chap. 4.
8. M. G. Grimaldi, F. Priolo, P. Baeri, and E. Rimini, *Phys. Rev. B* **35**:5117 (1987).
9. A. H. Van Ommen, C. W. T. Bulle-Lieuwma, and C. Langereis, *J. Appl. Phys.* **64**:2796 (1988).
10. M. O. Thompson, P. M. Bucksbaum, and J. Bokor, *Mat. Res. Symp. Proc.* **35**:435 (1985).